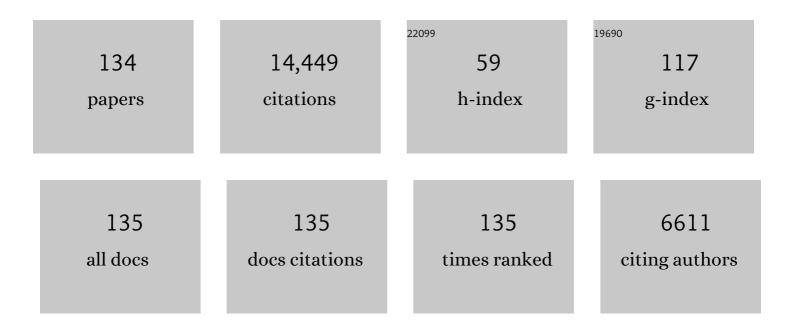
List of Publications by Year in descending order

Source: https://exaly.com/author-pdf/5448176/publications.pdf Version: 2024-02-01



DIDE PONC

#	Article	IF	CITATIONS
1	Mechanisms of austenite growth during intercritical annealing in medium manganese steels. Scripta Materialia, 2022, 206, 114228.	2.6	27
2	Hydrogen-assisted failure in Inconel 718 fabricated by laser powder bed fusion: The role of solidification substructure in the embrittlement. Scripta Materialia, 2022, 207, 114308.	2.6	20
3	On the influence of heavy warm reduction on the microstructure and mechanical properties of a medium-carbon ferritic –pearlitic steel. International Journal of Materials Research, 2022, 95, 1108-1114.	0.1	0
4	Strain hardening engineering via grain size control in laser powder-bed fusion. Materials Science & Engineering A: Structural Materials: Properties, Microstructure and Processing, 2022, 838, 142773.	2.6	1
5	Hydrogen trapping and embrittlement in high-strength Al alloys. Nature, 2022, 602, 437-441.	13.7	109
6	The dual role of martensitic transformation in fatigue crack growth. Proceedings of the National Academy of Sciences of the United States of America, 2022, 119, .	3.3	25
7	Making sustainable aluminum by recycling scrap: The science of "dirty―alloys. Progress in Materials Science, 2022, 128, 100947.	16.0	134
8	Effect of Nb micro-alloying on austenite nucleation and growth in a medium manganese steel during intercritical annealing. Acta Materialia, 2022, 229, 117786.	3.8	24
9	A sustainable ultra-high strength Fe18Mn3Ti maraging steel through controlled solute segregation and α-Mn nanoprecipitation. Nature Communications, 2022, 13, 2330.	5.8	22
10	High stress twinning in a compositionally complex steel of very high stacking fault energy. Nature Communications, 2022, 13, .	5.8	38
11	Beyond Solid Solution Highâ€Entropy Alloys: Tailoring Magnetic Properties via Spinodal Decomposition. Advanced Functional Materials, 2021, 31, 2007668.	7.8	51
12	Comparative study of hydrogen embrittlement resistance between additively and conventionally manufactured 304L austenitic stainless steels. Materials Science & Engineering A: Structural Materials: Properties, Microstructure and Processing, 2021, 803, 140499.	2.6	23
13	Microstructure and deformation behavior of two TWIP/TRIP high entropy alloys upon grain refinement. Materials Science & Engineering A: Structural Materials: Properties, Microstructure and Processing, 2021, 802, 140661.	2.6	30
14	Intercritical annealing to achieve a positive strain-rate sensitivity of mechanical properties and suppression of macroscopic plastic instabilities in multi-phase medium-Mn steels. Materials Science & Engineering A: Structural Materials: Properties, Microstructure and Processing, 2021, 803, 140469.	2.6	11
15	Current Challenges and Opportunities Toward Understanding Hydrogen Embrittlement Mechanisms in Advanced High-Strength Steels: A Review. Acta Metallurgica Sinica (English Letters), 2021, 34, 741-754.	1.5	54
16	Enhancement of the tensile properties and impact toughness of a medium-Mn steel through the homogeneous microstrain distribution. Materials Characterization, 2021, 174, 110992.	1.9	11
17	The hidden structure dependence of the chemical life of dislocations. Science Advances, 2021, 7, .	4.7	24
	<pre>cmml·math</pre>		

<mml:math xmlns:mml="http://www.w3.org/1998/Math/MathML"><mml:mrow><mml:mn>3</mml:mn><mml:mi>d</mml:mi>d</mml:mrow></mml:r transition-metal high-entropy Invar alloy developed by adjusting the valence-electron concentration. Physical Review Materials, 2021, 5, . 18

#	Article	IF	CITATIONS
19	Chemical heterogeneity enhances hydrogen resistance in high-strength steels. Nature Materials, 2021, 20, 1629-1634.	13.3	83
20	Ultrastrong and Ductile Soft Magnetic Highâ€Entropy Alloys via Coherent Ordered Nanoprecipitates. Advanced Materials, 2021, 33, e2102139.	11.1	69
21	Recrystallization kinetics, mechanisms, and topology in alloys processed by laser powder-bed fusion: AISI 316L stainless steel as example. Materialia, 2021, 20, 101236.	1.3	19
22	Localized deformation inside the Lüders front of a medium manganese steel. Materials Science & Engineering A: Structural Materials: Properties, Microstructure and Processing, 2021, 824, 141816.	2.6	25
23	Joint investigation of strain partitioning and chemical partitioning in ferrite-containing TRIP-assisted steels. Acta Materialia, 2020, 186, 374-388.	3.8	47
24	Reversible dislocation movement, martensitic transformation and nano-twinning during elastic cyclic loading of a metastable high entropy alloy. Acta Materialia, 2020, 185, 474-492.	3.8	48
25	Dependence of hydrogen embrittlement mechanisms on microstructure-driven hydrogen distribution in medium Mn steels. Acta Materialia, 2020, 183, 313-328.	3.8	78
26	On the mechanical heterogeneity in dual phase steel grades: Activation of slip systems and deformation of martensite in DP800. Acta Materialia, 2020, 183, 274-284.	3.8	71
27	Could face-centered cubic titanium in cold-rolled commercially-pure titanium only be a Ti-hydride?. Scripta Materialia, 2020, 178, 39-43.	2.6	36
28	In-situ synthesis via laser metal deposition of a lean Cu–3.4Cr–0.6Nb (at%) conductive alloy hardened by Cr nano-scale precipitates and by Laves phase micro-particles. Acta Materialia, 2020, 197, 330-340.	3.8	30
29	The impact of grain-scale strain localization on strain hardening of a high-Mn steel: Real-time tracking of the transition from the γÂ→ÂεÂ→Âα' transformation to twinning. Acta Materialia, 2020, 197, 123-136.	3.8	37
30	Ultrastrong lightweight compositionally complex steels via dual-nanoprecipitation. Science Advances, 2020, 6, .	4.7	118
31	Reversion and re-aging of a peak aged Al-Zn-Mg-Cu alloy. Scripta Materialia, 2020, 188, 269-273.	2.6	37
32	Formation mechanism of <mml:math <br="" xmlns:mml="http://www.w3.org/1998/Math/MathML">altimg="si1.svg"&gt;<mml:mi>l²</mml:mi></mml:math> -carbides and deformation behavior in Si-alloyed FeMnAlC lightweight steels. Acta Materialia, 2020, 198, 258-270.	3.8	54
33	Current Challenges and Opportunities in Microstructure-Related Properties of Advanced High-Strength Steels. Metallurgical and Materials Transactions A: Physical Metallurgy and Materials Science, 2020, 51, 5517-5586.	1.1	115
34	Phase boundary segregation-induced strengthening and discontinuous yielding in ultrafine-grained duplex medium-Mn steels. Acta Materialia, 2020, 200, 389-403.	3.8	70
35	Segregation-assisted spinodal and transient spinodal phase separation at grain boundaries. Npj Computational Materials, 2020, 6, .	3.5	29
36	High-rate superplasticity in an equiatomic medium-entropy VCoNi alloy enabled through dynamic recrystallization of a duplex microstructure of ordered phases. Acta Materialia, 2020, 194, 106-117.	3.8	57

#	Article	IF	CITATIONS
37	Interplay of Chemistry and Faceting at Grain Boundaries in a Model Al Alloy. Physical Review Letters, 2020, 124, 106102.	2.9	25
38	Chemical boundary engineering: A new route toward lean, ultrastrong yet ductile steels. Science Advances, 2020, 6, eaay1430.	4.7	120
39	(Al, Zn)3Zr dispersoids assisted η′ precipitation in anAl-Zn-Mg-Cu-Zr alloy. Materialia, 2020, 10, 100641.	1.3	28
40	Unveiling the mechanism of abnormal magnetic behavior of FeNiCoMnCu high-entropy alloys through a joint experimental-theoretical study. Physical Review Materials, 2020, 4, .	0.9	18
41	Grain boundary segregation and precipitation in an Al-Zn-Mg-Cu alloy. MATEC Web of Conferences, 2020, 326, 01004.	0.1	0
42	Experimental and numerical study of mechanical properties of multi-phase medium-Mn TWIP-TRIP steel: Influences of strain rateÂand phase constituents. Acta Materialia, 2019, 177, 250-265.	3.8	50
43	Macroscopic to nanoscopic in situ investigation on yielding mechanisms in ultrafine grained medium Mn steels: Role of the austenite-ferrite interface. Acta Materialia, 2019, 178, 10-25.	3.8	95
44	Quantification of solute deuterium in titanium deuteride by atom probe tomography with both laser pulsing and high-voltage pulsing: influence of the surface electric field. New Journal of Physics, 2019, 21, 053025.	1.2	26
45	Effect of volume fraction and mechanical stability of austenite on ductility of medium Mn steel. Journal of Iron and Steel Research International, 2019, 26, 1209-1218.	1.4	16
46	Ti and its alloys as examples of cryogenic focused ion beam milling of environmentally-sensitive materials. Nature Communications, 2019, 10, 942.	5.8	89
47	Metastability alloy design. MRS Bulletin, 2019, 44, 266-272.	1.7	36
48	Strain hardening mechanisms during cold rolling of a high-Mn steel: Interplay between submicron defects and microtexture. Materials Science & Engineering A: Structural Materials: Properties, Microstructure and Processing, 2019, 754, 636-649.	2.6	18
49	An Automated Computational Approach for Complete In-Plane Compositional Interface Analysis by Atom Probe Tomography. Microscopy and Microanalysis, 2019, 25, 389-400.	0.2	16
50	Thermodynamics of grain boundary segregation, interfacial spinodal and their relevance for nucleation during solid-solid phase transitions. Acta Materialia, 2019, 168, 109-120.	3.8	56
51	Improving the ductility of ultrahigh-strength medium Mn steels via introducing pre-existed austenite acting as a "reservoir―for Mn atoms. Materials Science & Engineering A: Structural Materials: Properties, Microstructure and Processing, 2019, 749, 235-240.	2.6	26
52	Strain partitioning and strain localization in medium manganese steels measured by in situ microscopic digital image correlation. Materialia, 2019, 5, 100252.	1.3	42
53	Martensite to austenite reversion in a high-Mn steel: Partitioning-dependent two-stage kinetics revealed by atom probe tomography, in-situ magnetic measurements and simulation. Acta Materialia, 2019, 166, 178-191.	3.8	27
54	Ultrastrong Mediumâ€Entropy Singleâ€Phase Alloys Designed via Severe Lattice Distortion. Advanced Materials, 2019, 31, e1807142.	11.1	301

#	Article	IF	CITATIONS
55	Carbon and strain partitioning in a quenched and partitioned steel containing ferrite. Acta Materialia, 2019, 165, 561-576.	3.8	75
56	Revealing fracture mechanisms of medium manganese steels with and without delta-ferrite. Acta Materialia, 2019, 164, 683-696.	3.8	108
57	Deformation compatibility between nanotwinned and recrystallized grains enhances resistance to interface cracking in cyclic loaded stainless steel. Acta Materialia, 2019, 165, 87-98.	3.8	39
58	Multi-scale characterization of austenite reversion and martensite recovery in a cold-rolled medium-Mn steel. Acta Materialia, 2019, 166, 512-530.	3.8	67
59	Atomic-scale investigation of hydrogen distribution in a Ti Mo alloy. Scripta Materialia, 2019, 162, 321-325.	2.6	18
60	Competition between formation of carbides and reversed austenite during tempering of a medium-manganese steel studied by thermodynamic-kinetic simulations and atom probe tomography. Acta Materialia, 2018, 147, 165-175.	3.8	60
61	Hydrogen embrittlement of an interstitial equimolar high-entropy alloy. Corrosion Science, 2018, 136, 403-408.	3.0	96
62	Phase nucleation through confined spinodal fluctuations at crystal defects evidenced in Fe-Mn alloys. Nature Communications, 2018, 9, 1137.	5.8	101
63	Characterizing solute hydrogen and hydrides in pure and alloyed titanium at the atomic scale. Acta Materialia, 2018, 150, 273-280.	3.8	81
64	Interfaces and defect composition at the near-atomic scale through atom probe tomography investigations. Journal of Materials Research, 2018, 33, 4018-4030.	1.2	35
65	Segregation assisted grain boundary precipitation in a model Al-Zn-Mg-Cu alloy. Acta Materialia, 2018, 156, 318-329.	3.8	189
66	On the origin of the improvement of shape memory effect by precipitating VC in Fe–Mn–Si-based shape memory alloys. Acta Materialia, 2018, 155, 222-235.	3.8	60
67	Reversion to Ultrafine-Grained Austenite in a Medium-Mn AHSS. Microscopy and Microanalysis, 2018, 24, 2228-2229.	0.2	0
68	Beating hydrogen with its own weapon: Nano-twin gradients enhance embrittlement resistance of a high-entropy alloy. Materials Today, 2018, 21, 1003-1009.	8.3	127
69	Parameter free quantitative analysis of atom probe data by correlation functions: Application to the precipitation in Al-Zn-Mg-Cu. Scripta Materialia, 2018, 154, 106-110.	2.6	55
70	Hydrogen-assisted failure in Ni-based superalloy 718 studied under in situ hydrogen charging: The role of localized deformation in crack propagation. Acta Materialia, 2017, 128, 365-374.	3.8	136
71	Bone-like crack resistance in hierarchical metastable nanolaminate steels. Science, 2017, 355, 1055-1057.	6.0	297
72	Ultrastrong steel via minimal lattice misfit and high-density nanoprecipitation. Nature, 2017, 544, 460-464.	13.7	843

#	Article	IF	CITATIONS
73	Superplasticity in a lean Fe-Mn-Al steel. Nature Communications, 2017, 8, 751.	5.8	51
74	Strengthening and strain hardening mechanisms in a precipitation-hardened high-Mn lightweight steel. Acta Materialia, 2017, 140, 258-273.	3.8	179
75	Characterization of Partitioning in a Medium-Mn Third-Generation AHSS. Microscopy and Microanalysis, 2017, 23, 402-403.	0.2	6
76	1 billion tons of nanostructure – segregation engineering enables confined transformation effects at lattice defects in steels. IOP Conference Series: Materials Science and Engineering, 2017, 219, 012006.	0.3	3
77	Improved Atom Probe Methodology for Studying Carbon Redistribution in Low-Carbon High-Ms Lath Martensitic Steels. Microscopy and Microanalysis, 2017, 23, 706-707.	0.2	4
78	Confined chemical and structural states at dislocations in Fe-9wt%Mn steels: A correlative TEM-atom probe study combined with multiscale modelling. Acta Materialia, 2017, 124, 305-315.	3.8	73
79	The effects of prior austenite grain boundaries and microstructural morphology on the impact toughness of intercritically annealed medium Mn steel. Acta Materialia, 2017, 122, 199-206.	3.8	196
80	Influence of Intercritical Annealing on Microstructure and Mechanical Properties of a Medium Manganese Steel. Procedia Engineering, 2017, 207, 1803-1808.	1.2	9
81	Strain hardening by dynamic slip band refinement in a high-Mn lightweight steel. Acta Materialia, 2016, 116, 188-199.	3.8	276
82	Spectral TRIP enables ductile 1.1ÂGPa martensite. Acta Materialia, 2016, 111, 262-272.	3.8	141
83	Effect of intercritical deformation on microstructure and mechanical properties of a low-silicon aluminum-added hot-rolled directly quenched and partitioned steel. Materials Science & Engineering A: Structural Materials: Properties, Microstructure and Processing, 2016, 656, 200-215.	2.6	29
84	Multi-scale and spatially resolved hydrogen mapping in a Ni–Nb model alloy reveals the role of the δ phase in hydrogen embrittlement of alloy 718. Acta Materialia, 2016, 109, 69-81.	3.8	116
85	Dynamic strain-induced transformation: An atomic scale investigation. Scripta Materialia, 2015, 109, 23-27.	2.6	30
86	Atom probe tomography reveals options for microstructural design of steels and titanium alloys by segregation engineering. MATEC Web of Conferences, 2015, 33, 01001.	0.1	0
87	Atomic scale investigation of non-equilibrium segregation of boron in a quenched Mo-free martensitic steel. Ultramicroscopy, 2015, 159, 240-247.	0.8	40
88	Grain boundary segregation engineering and austenite reversion turn embrittlement into toughness: Example of a 9 wt.% medium Mn steel. Acta Materialia, 2015, 86, 182-192.	3.8	229
89	3D structural and atomic-scale analysis of lath martensite: Effect of the transformation sequence. Acta Materialia, 2015, 95, 366-377.	3.8	191
90	An Overview of Dual-Phase Steels: Advances in Microstructure-Oriented Processing and Micromechanically Guided Design. Annual Review of Materials Research, 2015, 45, 391-431.	4.3	469

#	Article	IF	CITATIONS
91	Enhancing Hydrogen Embrittlement Resistance of Lath Martensite by Introducing Nano-Films of Interlath Austenite. Metallurgical and Materials Transactions A: Physical Metallurgy and Materials Science, 2015, 46, 3797-3802.	1.1	77
92	Linear complexions: Confined chemical and structural states at dislocations. Science, 2015, 349, 1080-1083.	6.0	227
93	Nanolaminate transformation-induced plasticity–twinning-induced plasticity steel with dynamic strain partitioning and enhanced damage resistance. Acta Materialia, 2015, 85, 216-228.	3.8	207
94	Segregation of boron at prior austenite grain boundaries in a quenched martensitic steel studied by atom probe tomography. Scripta Materialia, 2015, 96, 13-16.	2.6	81
95	Mechanisms of subgrain coarsening and its effect on the mechanical properties of carbon-supersaturated nanocrystalline hypereutectoid steel. Acta Materialia, 2015, 84, 110-123.	3.8	60
96	Enhanced superplasticity in an Al-alloyed multicomponent Mn–Si–Cr–C steel. Acta Materialia, 2014, 63, 232-244.	3.8	34
97	Designing quadplex (four-phase) microstructures in an ultrahigh carbon steel. Materials Science & Engineering A: Structural Materials: Properties, Microstructure and Processing, 2014, 612, 46-53.	2.6	12
98	Smaller is less stable: Size effects on twinning vs. transformation of reverted austenite in TRIP-maraging steels. Acta Materialia, 2014, 79, 268-281.	3.8	225
99	Grain boundary segregation engineering in metallic alloys: A pathway to the design of interfaces. Current Opinion in Solid State and Materials Science, 2014, 18, 253-261.	5.6	466
100	New insights into the austenitization process of low-alloyed hypereutectoid steels: Nucleation analysis of strain-induced austenite formation. Acta Materialia, 2014, 80, 296-308.	3.8	19
101	Designing Heusler nanoprecipitates by elastic misfit stabilization in Fe–Mn maraging steels. Acta Materialia, 2014, 76, 94-105.	3.8	65
102	Superplastic Mn–Si–Cr–C duplex and triplex steels: Interaction of microstructure and void formation. Materials Science & Engineering A: Structural Materials: Properties, Microstructure and Processing, 2014, 610, 355-369.	2.6	12
103	Segregation engineering enables nanoscale martensite to austenite phase transformation at grain boundaries: A pathway to ductile martensite. Acta Materialia, 2013, 61, 6132-6152.	3.8	264
104	Inheritance of Dislocations and Crystallographic Texture during Martensitic Reversion into Austenite. ISIJ International, 2013, 53, 1286-1288.	0.6	33
105	Transition from Diffusive to Displacive Austenite Reversion in Low-Alloy Steel. ISIJ International, 2013, 53, 2275-2277.	0.6	31
106	New Insights into the Atomic-Scale Structures and Behavior of Steels. Microscopy Today, 2012, 20, 44-48.	0.2	32
107	Microstructure Control during Fabrication of Ultrafine Grained Dual-phase Steel: Characterization and Effect of Intercritical Annealing Parameters. ISIJ International, 2012, 52, 874-883.	0.6	65
108	Nanoscale austenite reversion through partitioning, segregation and kinetic freezing: Example of a ductile 2GPa Fe–Cr–C steel. Acta Materialia, 2012, 60, 2790-2804.	3.8	167

#	Article	IF	CITATIONS
109	On the Effect of Manganese on Grain Size Stability and Hardenability in Ultrafine-Grained Ferrite/Martensite Dual-Phase Steels. Metallurgical and Materials Transactions A: Physical Metallurgy and Materials Science, 2012, 43, 37-46.	1.1	116
110	Design of Lean Maraging TRIP Steels. , 2011, , 199-208.		4
111	Design of a novel Mn-based 1GPa duplex stainless TRIP steel with 60% ductility by a reduction of austenite stability. Acta Materialia, 2011, 59, 4653-4664.	3.8	422
112	Characterization of Nanoâ€Sized Precipitates in a Mnâ€Based Lean Maraging Steel by Atom Probe Tomography. Steel Research International, 2011, 82, 137-145.	1.0	13
113	Chemical gradients across phase boundaries between martensite and austenite in steel studied by atom probe tomography and simulation. Acta Materialia, 2011, 59, 364-374.	3.8	255
114	Deformation and fracture mechanisms in fine- and ultrafine-grained ferrite/martensite dual-phase steels and the effect of aging. Acta Materialia, 2011, 59, 658-670.	3.8	618
115	Pulsed-laser atom probe studies of a precipitation hardened maraging TRIP steel. Ultramicroscopy, 2011, 111, 623-627.	0.8	22
116	Effect of grain refinement to 1μm on strength and toughness of dual-phase steels. Materials Science & Engineering A: Structural Materials: Properties, Microstructure and Processing, 2010, 527, 7832-7840.	2.6	294
117	Orientation gradients and geometrically necessary dislocations in ultrafine grained dual-phase steels studied by 2D and 3D EBSD. Materials Science & Engineering A: Structural Materials: Properties, Microstructure and Processing, 2010, 527, 2738-2746.	2.6	1,482
118	Nanoprecipitate-hardened 1.5GPa steels with unexpected high ductility. Scripta Materialia, 2009, 60, 1141-1144.	2.6	248
119	Designing Ultrahigh Strength Steels with Good Ductility by Combining Transformation Induced Plasticity and Martensite Aging. Advanced Engineering Materials, 2009, 11, 547-555.	1.6	99
120	Ultrafine Grained Ferrite/Martensite Dual Phase Steel Fabricated by Large Strain Warm Deformation and Subsequent Intercritical Annealing. ISIJ International, 2008, 48, 1096-1101.	0.6	66
121	Characterization of the Microstructure, Crystallographic Texture and Segregation of an Asâ€cast Duplex Stainless Steel Slab. Steel Research International, 2008, 79, 482-488.	1.0	30
122	Investigation of Orientation Gradients in Pearlite in Hypoeutectoid Steel by use of Orientation Imaging Microscopy. Steel Research International, 2007, 78, 38-44.	1.0	45
123	Design of high-strength steels by microalloying and thermomechanical treatment. Materials Science & Engineering A: Structural Materials: Properties, Microstructure and Processing, 2007, 463, 138-146.	2.6	74
124	Austenite Grain Coarsening Behaviour in a Medium Carbon Si-Cr Spring Steel with and without Vanadium. Steel Research International, 2006, 77, 590-594.	1.0	2
125	Refinement of grain boundary carbides in a Si–Cr spring steel by thermomechanical treatment. Materials Science & Engineering A: Structural Materials: Properties, Microstructure and Processing, 2006, 426, 194-201.	2.6	36
126	Overview of processing, microstructure and mechanical properties of ultrafine grained bcc steels. Materials Science & Engineering A: Structural Materials: Properties, Microstructure and Processing, 2006, 441, 1-17.	2.6	498

#	Article	IF	CITATIONS
127	Microstructure and crystallographic texture of an ultrafine grained C–Mn steel and their evolution during warm deformation and annealing. Acta Materialia, 2005, 53, 845-858.	3.8	264
128	Mechanical properties of an ultrafine grained C–Mn steel processed by warm deformation and annealing. Acta Materialia, 2005, 53, 4881-4892.	3.8	299
129	Improvement of the work hardening rate of ultrafine grained steels through second phase particles. Scripta Materialia, 2005, 52, 1075-1080.	2.6	208
130	Influence of Mn Content on the Microstructure and Mechanical Properties of Ultrafine Grained C-Mn Steels. ISIJ International, 2005, 45, 1721-1726.	0.6	35
131	On the influence of heavy warm reduction on the microstructure and mechanical properties of a medium-carbon ferritic–pearlitic steel. International Journal of Materials Research, 2004, 95, 1108-1114.	0.8	6
132	Grain boundary characterization and grain size measurement in an ultrafine-grained steel. International Journal of Materials Research, 2004, 95, 513-517.	0.8	23
133	Development of microstructure and texture of medium carbon steel during heavy warm deformation. Acta Materialia, 2004, 52, 2209-2220.	3.8	146
134	The Microstructure and Mechanical Properties of Ultrafine Grained Plain C-Mn Steels. Steel Research International, 2004, 75, 33-37.	1.0	11